An Analytical Channel Model for Emerging Wireless Networks-on-Chip

Michael Opoku Agyeman[1], Quoc-Tuan Vien[2], Terrence Mak[3]

[1]Department of Computer and Immersive Technologies, University of Northampton, Email: Michael.OpokuAgyeman@northampton.ac.uk
[2]School of Science and Technology, Middlesex University, London, UK, Email: Q.Vien@mdx.ac.uk
[3]ECS, Faculty of Physical Sciences and Engineering, University of Southampton, Email: tmak@ecs.soton.ac.uk

Abstract—Recently wireless Networks-on-Chip (WiNoCs) have been proposed to overcome the scalability and performance limitations of traditional multi-hop wired NoC architectures. However, the adaptation of wireless technology for on-chip communication is still in its infancy. Consequently, several challenges such as simulation and design tools that consider the technological constraints imposed by the wireless channel are yet to be addressed. To this end, in this paper, we propose and efficient channel model for WiNoCs which takes into account practical issues and constraints of the propagation medium, such as transmission frequency, operating temperature, ambient pressure and distance between the on-chip antennas. The proposed channel model demonstrates that total path loss of the wireless channel in WiNoCs suffers from not only dielectric propagation loss (DPL) but also molecular absorption attenuation (MAA) which reduces the reliability of the system.

I. INTRODUCTION

Recently, System-on-Chip (SoC) has emerged to combine several components such as processors, peripherals, memory blocks and power management circuits on a single integrated circuit (IC) as one of the most interesting solutions in embedded applications [1]. A dominant issue with next generation multi-core design arises from the nonscalable wire delays and power consumption of the on-chip communication infrastructure. These issues have attracted a lot of research over the past few years, such as the maximum number of cores per shared bus, efficient application mapping, reliability and efficient arbitration for accessing shared bus. To compensate for the fast-paced technological scalability with the performance bottleneck of conventional metal based interconnects (wireline), the research for alternative interconnect fabrics such as optical networks, three dimensional integrated circuits (3-D ICs) and millimeter wave (mm-wave) has emerged for SoC design [1]–[6]. In optical interconnects a photon needs to be converted back to electrons to be stored in the electronic circuitry. Consequently, optical networks have a high design complexity as well as high power, area, and latency overheads. On the other hand, though 3-D ICs are Complementary Metal Oxide Semiconductor (CMOS) compatible and have shorter vertical links with enhanced scalability, 3D integration is still in its infancy due to alignment, low yield and high temperature dissipation issues in the current technology which lowers the reliability of system [7]–[9].

RF interconnect has low area and low power consumption due to its CMOS compatibility. However, RF interconnect relies on long transmission lines for guided data transmission which requires alignment between transmission pairs. Mm-Wave, has emerged as a more feasible solution with promising CMOS components that can scale with transistor technology. Consequently, Wireless Network-on-Chip (NoC) has been proposed as a more promising solution to these issues and has gained the attention of many researchers in this field of study [10]. WiNoCs adopt mm-Wave enabled routers and packet or circuit switching to handle data communication in a multi-core system. Recent research shows that WiNoCs outperforms its more conventional wired counterpart [11] with low power consumption and reduced latency between remote cores. However, WiNoC is still in its infancy and several challenges are currently being addressed to facilitate its acceptance as a mainstream interconnect fabric and bridge the widening gap between computation complexity and communication efficiency for emerging SoC design [10]. Particularly, new design evaluation tools must account for the constraints imposed by the wireless interface. Compared to wireline NoCs, the critical difference is the model of wireless propagation channel in WiNoCs.

In order to more accurately simulate and evaluate the actual performance of system, a wireless propagation channel model is required. In this paper, We propose a parameterizable wireless channel model to evaluate the losses in emerging WiNoCs. Considering both line-of-sight and reflective transmission in traditional WiNoCs an on-chip reflection channel model which accounts for the transmission medium and built-in material of a practical chip is developed. Simulation results of the proposed channel model reveals that, the performance degradation due to separation distance between on-chip antennas is higher with low reliability compared to a conventional channel modeled over DPL space. We demonstrate that, the total path loss of the signal transmission consists of both dielectric propagation loss (DPL) and molecular absorption attenuation (MAA). As a second contribution of the paper, we evaluate the effects of the medium compositions within the chip package on the total noise temperature of a WiNoC. The noise temperature and path loss model caused by the molecular absorption are shown to have a significant impact on the capacity of the WiNoC. It is also observed that transmission along the wireless channel in WiNoCs is less efficient compared to conventional wireless channel model with no MAA, even when the transmission distance between two antennas is very small (less than 0.01 mm).

The rest of the paper is organized as follows. Section II presents current contributions on WiNoCs. Section III evaluates the performance effect of wireless channel on NoCs. Sections IV and V present the system model and propose a parameterizable channel model for WiNoCs, respectively. Experimental result in Section VI validates the significance

of the proposed channel model. Finally, the main findings are concluded in Section VII.

II. RELATED WORK

One of the key problems with WiNoCs identified in [12] is the transmission reliability of the wireless channel. As an effort to address this issue, Ganguly et al. [13] proposed an error control coding for WiNoCs. By implementing a joint crosstalk triple error correction and simultaneous quadruple error detection codes in the wire line links and Hamming code-based product codes in the wireless links with Carbon Nanotube (CNT) antennas, it was demonstrated that, the reliability of the wireless channel could be improved. Similarly, ECC has been adapted in [11] to improve the reliability of WiNoCs. However, ECC introduces timing, area and packet overheads which affects the overall transmission efficiency of the WiNoC [14]. Alternatively, Lee et al. [14] adopted an overhearing scheme for WiNoCs. Here a zero-signaling-overhearing-and-retransmission is presented to manage the packet loss along the wireless channel. A checksum-based error-detection and retransmission scheme at the last hop. Vijayakumaran et al. [15] presented an improved filter design to enhance the performance as well as reduce the error probability of incurred by synchronization delays in CDMA based WiNoCs. However, these techniques rely on the underlying lossy wireless communication fabric for retransmission of handshake signals, erroneous and non-erroneous packets.

In order to accurately model the reliability of the wireless channel in WiNoCs for simulation and evaluation, a parameterizable channel model that considers the on-chip constraints is required. Among the key challenges of the channel modeling for WiNoC presented in [16], it is emphasized that no comprehensive work on on-chip channel modeling has been reported. Therefore, considering the deployment of antennas operating in the GHz band in a practical chip, the contribution of the paper is to investigate the effects of various on-chip propagation constraints on the performance of WiNoCs.

III. EFFECT OF WIRELESS CHANNEL ON NOCS

To demonstrate the effect of wireless channel on the performance of NoCs, we have performed simulations in Ansys High Frequency Structured Simulator [17]. Here, a zigzag antennas which is considered to be the most efficient antenna for mm-Wave on-chip communication is employed. The zigzag antennas are separated by a distance of only 20mm.

Fig. 1 compares the S_{21} (dB) of different technologies. It can be seen that, the S_{21} of mm-Wave is around -36dB which is significantly lower than that of the wireline communication fabric. Moreover, though wireline can achieve a high signal strength, its transmission frequency is inhibited by induced coupling, crosstalk and temperature induced noises [13]. Consequently, when employed as the wireless communication medium for WiNoCs, the high BER of mm-Wave reduces the reliability of the NoC. Fig. 2 shows that, for a fixed signal to noise ratio (SNR) of a communication fabric with an attenuation constant α, the improvement in rate of change in transmission gain $G_{a,dB}$ for a receiver node placed at $d^{'}$
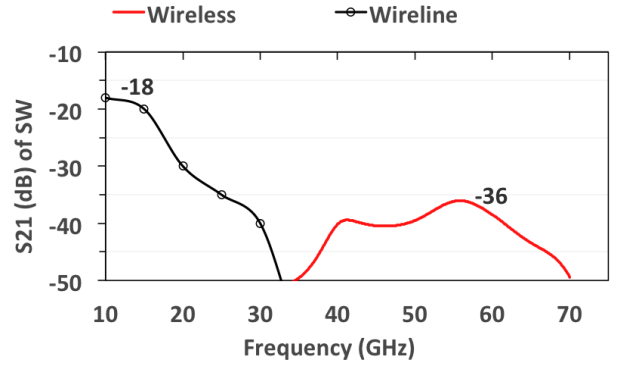

Fig. 1. S_{21} (dB) over wide-band frequency on the reactive surface

from a transmitting node at d which is given by:

$$G_{a,dB} = \frac{-20}{T_{(d^{'}-d),ps}} \left(\log_{10} \left(\frac{d^{'}}{d} \right) + \alpha(d^{'} - d) \log_{10} e \right) \quad (1)$$

of mm-Wave over wireline increases significantly as the separation between transmitting node and receive node increases. In the wireline channels, there is no need for transceiver circuits to convert wireless signals. Hence at low distances, wireline is more efficient than the wireless communication fabric. However, the delay along the wires have drastic effects which cause significant drop in the rate of transmission gain as the distance to destination node increases. Therefore in
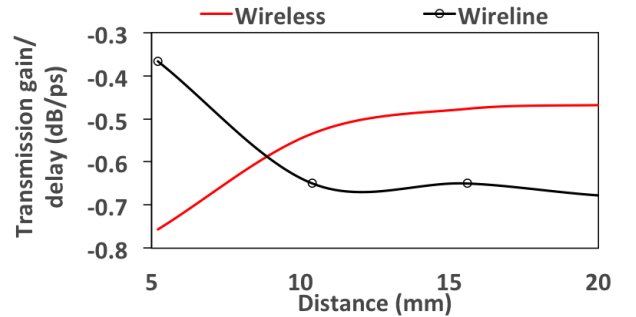

Fig. 2. Variation of ratio of rate of change of transmission gain with distance for different on-chip communication medium

this paper, a wireless channel model is proposed to analyse the transmission loss components in order to evaluate the reliability of WiNoCs.

IV. ON-CHIP WIRELESS SIGNAL PROPAGATION

In order to understand the reduction in performance of WiNoCs due to the reliability issues of wireless channel, it is important to characterize the traditional mm-Wave transmission channel for on-chip wireless communication.

Fig. 3 illustrates a typical WiNoC architecture where two cores $\mathcal{C}_{\mathcal{T}}$ and $\mathcal{C}_{\mathcal{R}}$ the transmitter and receiver cores, respectively, communicate via mm-Wave channel. Here, we consider a metal cube enclosure as the package with a longest rectangular side of d_C and a height of $h \ll d_C$. Let h_T
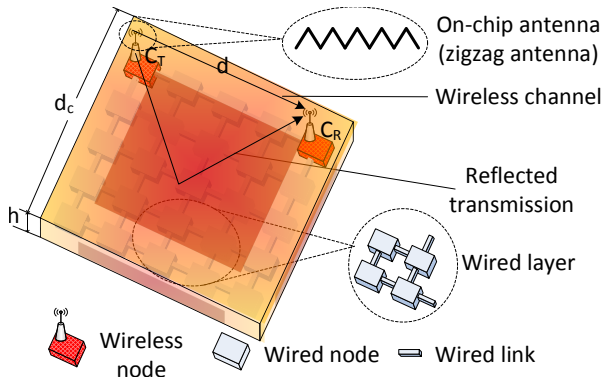
Fig. 3. System model of the communication between two cores in existing hybrid wired-wireless Network-on-Chip

and h_R denote the height of the mm-Wave antennas (zigzag antennas) at C_T and C_R, respectively. The material property of the transmission medium between C_T and C_R is assumed to be time-invariant over the transmission of a data frame and changes independently from one frame to another"[1]". Let d denote the distance of separation between C_T and C_R. Accounting for chip floorplanning and hence in order to avoid the placement of the cores on/near the edges of the package, d should be less than $d_{\max} = d_C\sqrt{2}$. To accurately model the wireless channel interface of existing WiNoCs, the absorption and resonance of the medium compositions within the chip package should be taken into account, especially in the high frequency band of modern multi-core design. Specifically, various molecules and their isotopologues may cause molecular absorption attenuation (MAA) at various frequency bands [18]. Therefore, the signal transmission between C_T and C_R in Fig. 3 suffers from the path loss caused by not only the dielectric propagation loss (DPL) but also the MAA.

For convenience, the main notation and the well-known constants used in this paper are listed in Tables I and II, respectively.

V. PROPOSED WIRELESS CHANNEL MODEL

We evaluate the wireless communication fabric for existing WiNoC. Unlike the conventional channel models for the macro-world, on-chip communication introduces new constraints and challenges. Hence in order to study the effect of the wireless channel on the performance of on-chip communication, we propose a channel model that considers the physical dynamics of multi-core communication. In the proposed channel model, the total path loss of electromagnetic signal transmission from C_T to C_R within the chip package consists of DPL and MAA.

A. Dielectric Propagation Loss (DPL)

It can be observed in Fig. 3 that the data transmission between two cores can be carried out via both direct line-of-sight (LoS) and reflected transmission. Therefore, in this paper,

---

[1]Note that there are various molecules of the gas within the material substance which may change over time. For simplicity, we consider quasi-static channel model in this work.

TABLE I.   SUMMARY OF NOTATION

Notation	Meaning
d [m]	distance between two mm-Wave antennas
d_C [m]	longest rectangular side of the chip package
d_0 [m]	reference distance
h [m]	height of the chip package
h_T, h_R [m]	elevation of the mm-Wave antennas at C_T, C_R, respectively
f [Hz]	transmission frequency
B [Hz]	channel bandwidth
p [atm]	ambient pressure applied on chip
$p_0 = 1$ atm	reference pressure
T_S [K]	system electronic noise temperature
T_M [K]	molecular absorption noise temperature
T' [K]	other noise source temperature
$T_p = 273.15$ K	temperature at standard pressure
$T_0 = 296$ K	reference temperature
L_s, L_a, L	DPL, MAA, total path loss, respectively
E_L, E_R [V/m]	line-of-sight, reflected components of E-field
E_0, E_T [V/m]	dielctric/free-space, total received E-field
θ [rad]	phase difference between E_L and E_R
P_T, P_R [W]	transmitted power, received power
G_T, G_R	transmitter antenna gain, receiver antenna gain
τ	transmittance of a medium
κ	medium absorption coefficient
(i, g)	isotopologue i of gas g
$\kappa^{(i,g)}$	individual absorption coefficient of (i, g)
$Q^{(i,g)}$ [mol/m^3]	molecular volumetric density of (i, g)
$\varsigma^{(i,g)}$ [m^2/mol]	absorption cross section of (i, g)
$q^{((i,g))}$ [%]	mixing ratio of (i, g)
$S^{(i,g)}$ [m^{2}Hz/mol]	line density for the absorption of (i, g)
$\xi^{(i,g)}$ [Hz^{-1}]	spectral line shape of (i, g)
$f_c^{(i,g)}$ [Hz]	resonant frequency of (i, g)
$f_{c_0}^{(i,g)}$ [Hz]	resonant frequency of (i, g) at $p_0 = 1$ atm
$v^{(i,g)}$ [Hz^{-1}]	Van Vleck-Weisskopf asymmetric line shape [19]
$\delta^{(i,g)}$ [Hz]	linear pressure shift of (i, g)
$\alpha_L^{(i,g)}$ [Hz]	Lorentz half-width of (i, g) [19]
α_0 [Hz]	broadening coefficient of air
$\beta^{(i,g)}$ [Hz]	broadening coefficient of (i, g)
ω	temperature broadening coefficient

TABLE II.   LIST OF CONSTANTS

Constant name	Symbol	Value
Avogadro constant	ζ_A	6.0221×10^{23} mol^{-1}
Boltzmann constant	ζ_B	1.3806×10^{-23} J/K
Gas constant	ζ_G	8.2051×10^{-5} m^{3}atm/K/mol
Light speed constant	ζ_L	2.9979×10^8 m/s
Planck constant	ζ_P	6.6262×10^{-34} Js

we develop a two-ray within-package reflection mode mm-Wave NoCs where the total received E-field $E_T(d, f)$ [V/m] at C_T consists of the LoS component $E_L(d, f)$ [V/m] and the reflected component $E_R(d, f)$ [V/m]. Summing up these two components, we have

$$\begin{aligned}
|E_T(d, f)| &= |E_L(d, f) + E_R(d, f)| \\
&= 2\frac{E_0 d_0}{d} \sin\left(\frac{\theta(d, f)}{2}\right),
\end{aligned} \quad (2)$$

where E_0 [V/m] is the dielectric E-field at a reference distance d_0 [m] and $\theta(d, f)$ [rad] is the phase difference between the two E-field components. Here, $\theta(d, f)$ can be approximated

by [20]

$$\theta(d, f) \approx \frac{4\pi h_T h_R f}{\zeta_L d}, \tag{3}$$

where h_T [m] and h_R [m] denote the height of the antennas at $\mathcal{C}_\mathcal{T}$ and $\mathcal{C}_\mathcal{R}$, respectively, and $\zeta_L = 2.9979 \times 10^8$ m/s is the speed of light in the vacuum.
From (2) and (3), the received power $P_R(d, f)$ [W] at $\mathcal{C}_\mathcal{R}$ can be computed by

$$\begin{aligned} P_R(d, f) &= \frac{|E_T(d, f)|^2 G_R \zeta_L^2}{480\pi^2 f^2} \\ &= \frac{E_0^2 d_0^2 \zeta_L^2}{120\pi^2 d^2 f^2} G_R \sin^2\left(\frac{2\pi h_T h_R f}{\zeta_L d}\right), \end{aligned} \tag{4}$$

where G_R denotes the antenna gain at $\mathcal{C}_\mathcal{R}$. Note that the equivalent isotropically radiated power (EIRP) is given by

$$\text{EIRP} = P_T G_T = \frac{E_0^2 d_0^2 4\pi}{120\pi} = \frac{E_0^2 d_0^2}{30}, \tag{5}$$

where P_T [W] and G_T denote the transmitted power and gain of the mm-Wave antenna at $\mathcal{C}_\mathcal{T}$, respectively. From (4) and (5), P_R can be given by

$$P_R(d, f) = \frac{P_T G_T G_R}{\left(\frac{2\pi d f}{\zeta_L}\right)^2} \sin^2\left(\frac{2\pi h_T h_R f}{\zeta_L d}\right). \tag{6}$$

Therefore, the DPL between $\mathcal{C}_\mathcal{T}$ and $\mathcal{C}_\mathcal{R}$ (i.e. $L_s(f, d)$) is obtained by

$$L_s(f, d) = \left(\frac{2\pi d f}{\zeta_L}\right)^2 \frac{1}{G_T G_R} \csc^2\left(\frac{2\pi h_T h_R f}{\zeta_L d}\right). \tag{7}$$

B. Molecular Absorption Attenuation (MAA)

The transmission of electromagnetic waves at frequency f through a transmission medium of distance d introduces MAA due to various molecules within the material substance. Applying Beer-Lambert's law to atmospheric measurements, the MAA of the data transmission from $\mathcal{C}_\mathcal{T}$ to $\mathcal{C}_\mathcal{R}$ (i.e. $L_a(f, d)$) can be determined by:

$$L_a(f, d) = \frac{1}{\tau(f, d)} = e^{\kappa(f)d}, \tag{8}$$

where $\tau(f, d)$ and $\kappa(f)$ [m^{-1}] are the transmittance and absorption coefficient of the medium, respectively. Here, $\kappa(f)$ depends on the composition of the medium (i.e. particular mixture of molecules along the channel) and it is given by:

$$\kappa(f) = \sum_{i,g} \kappa^{(i,g)}(f), \tag{9}$$

where $\kappa^{(i,g)}(f)$ [m^{-1}] denotes the individual absorption coefficient for the isotopologue i of gas g. For simplicity in representation, the isotopologue i of gas g is hereafter denoted by (i, g).
Applying radiative transfer theory [21], $\kappa^{(i,g)}(f)$ can be determined by

$$\kappa^{(i,g)}(f) = \frac{p}{p_0} \frac{T_p}{T_S} Q^{(i,g)} \varsigma^{(i,g)}(f), \tag{10}$$

where p [atm] is the ambient pressure applied on the designed SoC, T_S [K] is the system electronic noise temperature,

$p_0 = 1$ atm is the reference pressure, $T_p = 273.15$ K is the temperature at standard pressure, $Q^{(i,g)}$ [mol/m^3] is the molecular volumetric density (i.e. number of molecules per volume unit of (i, g)) and $\varsigma^{(i,g)}(f)$ [m^2/mol] is the absorption cross section of (i, g). Here, $Q^{(i,g)}$ is obtained by the Ideal Gas Law as

$$Q^{(i,g)} = \frac{p}{\zeta_G T_S} q^{(i,g)} \zeta_A, \tag{11}$$

where $\zeta_G = 8.2051 * 10^{-5}$ m^{3}atm/K/mol is the Gas constant, $\zeta_A = 6.0221 * 10^{23}$ mol^{-1} is the Avogadro constant and $q^{(i,g)}$ [%] is the mixing ratio of (i, g).
In (10), $\varsigma^{(i,g)}(f)$ is given by

$$\varsigma^{(i,g)(f)} = S^{(i,g)} \xi^{(i,g)}(f), \tag{12}$$

where $S^{(i,g)}$ [m^{2}Hz/mol] is the line density for the absorption of (i, g) (i.e. the absorption peak amplitude of (i, g)) and $\xi^{(i,g)}(f)$ [Hz^{-1}] is spectral line shape of (i, g) determined by

$$\xi^{(i,g)}(f) = \frac{f}{f_c^{(i,g)}} \frac{\tanh\left(\frac{\zeta_P \zeta_L f}{2\zeta_B T_S}\right)}{\tanh\left(\frac{\zeta_P f_c^{(i,g)}}{2\zeta_B T_S}\right)} v^{(i,g)}(f), \tag{13}$$

where $f_c^{(i,g)}$ [Hz] is the resonant frequency of (i, g), $\zeta_P = 6.6262 * 10^{-34}$ Js is the Planck constant, $\zeta_B = 1.3806 * 10^{-23}$ J/K is the Boltzmann constant and $v^{(i,g)}(f)$ [Hz^{-1}] is the Van Vleck-Weisskopf asymmetric line shape of (i, g). In (13),

$$f_c^{(i,g)} = f_{c_0}^{(i,g)} + \delta^{(i,g)} \frac{p}{p_0}, \tag{14}$$

where $f_{c_0}^{(i,g)}$ [Hz] is the resonant frequency of (i, g) at reference pressure $p_0 = 1$ atm and $\delta^{(i,g)}$ [Hz] is the linear pressure shift of (i, g). Also, the Van Vleck-Weisskopf asymmetric line shape of (i, g) in (13) is given by

$$\begin{aligned} v^{(i,g)}(f) = 100\zeta_L \frac{\alpha_L^{(i,g)}}{\pi} \frac{f}{f_c^{(i,g)}} &\left[\frac{1}{(f - f_c^{(i,g)})^2 + (\alpha_L^{(i,g)})^2} \right. \\ &\left. + \frac{1}{(f + f_c^{(i,g)})^2 + (\alpha_L^{(i,g)})^2} \right], \end{aligned} \tag{15}$$

where $\alpha_L^{(i,g)}$ [Hz] is the Lorentz half-width of (i, g). Here, $\alpha_L^{(i,g)}$ is computed by

$$\alpha_L^{(i,g)} = \left[(1 - q^{(i,g)})\alpha_0 + q^{(i,g)}\beta^{(i,g)}\right] \frac{p}{p_0} \left(\frac{T_0}{T_S}\right)^\omega, \tag{16}$$

where α_0 [Hz] is the broadening coefficient of air, $\beta^{(i,g)}$ [Hz] is the broadening coefficient of (i, g), $T_0 = 296$ K is the reference temperature and ω is the temperature broadening coefficient. Let $L(f, d)$ denote the total path loss for signal transmission at frequency f [Hz] over distance d [m]. From (7), (8) and (9), the total path loss of the proposed channel model is

$$\begin{aligned} L(f, d) &= L_s(f, d) L_a(f, d) \\ &= \left(\frac{2\pi d f}{\zeta_L}\right)^2 \frac{1}{G_T G_R} \csc^2\left(\frac{2\pi h_T h_R f}{\zeta_L d}\right) \prod_{i,g} e^{\kappa^{(i,g)}(f)d}. \end{aligned} \tag{17}$$

Remark 1 (Effectiveness of the proposed channel model)**.** In (17), it can be shown that $\kappa^{(i,g)} \geqslant 0 \ \forall i, g$. This means

the proposed channel model always has a higher total path loss than the conventional channel model with no MAA, and thus can represent the practical scenario as a performance benchmark.

Remark 2 (Environment-aware channel model)**.** The proposed channel model depends on not only the distance between two cores $\mathcal{C}_\mathcal{T}$ and $\mathcal{C}_\mathcal{R}$ but also the absorption of gas molecules, the temperature and the ambient pressure applied on the chip. In fact, from (10) - (16), the individual absorption coefficient for the isotopologue i of gas g (i.e. $\kappa^{(i,g)}(f)$) is shown to be dependent but not monotonically varied over the frequency.

C. Channel capacity of WiNoCs

We analyze the channel capacity of the wireless channel of WiNoCs with respect to the proposed channel model where the following observations could be made:

Lemma 1. *The channel capacity in bits/s of a nanocommunication system between two on-chip antennas is obtained by*

$$
\begin{aligned}
C(P_T, d) = \sum_{k=1}^{K} \Delta f \log_2 &\left[1 + \frac{P_T G_T G_R \sin^2\left(\frac{2\pi h_T h_R f_k}{\zeta_L d}\right)}{\zeta_B \left(\frac{2\pi d f_k}{\zeta_L}\right)^2 \Delta f} \right. \\
&\left. \times \frac{1}{(T_S + T_0)\prod_{i,g} e^{\kappa^{(i,g)}(f_k)d} - T_0} \right],
\end{aligned}
\tag{18}
$$

where K is the number of sub-bands in the total channel bandwidth of B [Hz], $\Delta f = B/K$ [Hz] is the width of each sub-band and f_k [Hz] is the center frequency of the k-th sub-band.

Proof: As the signal-to-noise ratio (SNR) is required for evaluating the achievable capacity of a communications system, we first derive the total noise power of the nanocommunications between two mm-Wave antennas. At frequency f [Hz], the total noise temperature at $\mathcal{C}_\mathcal{R}$ located at d [m] from $\mathcal{C}_\mathcal{T}$ (i.e. $T_{tot}(f,d)$ [K]) consists of the system electronic noise temperature (i.e. T_S [K]), the molecular absorption noise temperature (i.e. $T_M(f,d)$ [K]) and other noise source temperature (i.e. T' [K]), i.e.

$$
T_{tot}(f, d) = T_S + T_M(f, d) + T'. \tag{19}
$$

Assuming that $T_S + T_M(f,d) \gg T' \; \forall f, d$, we have

$$
T_{tot}(f, d) \approx T_S + T_M(f, d). \tag{20}
$$

Here, $T_M(f,d)$ is caused by the molecules within transmission medium, and thus can be expressed via the transmittance of the medium as

$$
T_M(f, d) = T_0(1 - \tau(f, d)) = T_0 \left(1 - \prod_{i,g} e^{-\kappa^{(i,g)}(f)d} \right). \tag{21}
$$

Substituting (21) into (20), we obtain

$$
T_{tot}(f, d) \approx T_S + T_0 \left(1 - \prod_{i,g} e^{-\kappa^{(i,g)}(f)d} \right). \tag{22}
$$

The total noise power at $\mathcal{C}_\mathcal{R}$ given transmission bandwidth B is therefore given by

$$
P_N(d) = \zeta_B \int_B T_{tot}(f, d) df. \tag{23}
$$

Note that the wireless channel for on-chip communication is highly frequency-selective and the molecular absorption noise is non-white. Therefore, we can divide the total bandwidth B into K narrow sub-bands to evaluate the capacity, in bits/s, as follows:

$$
C(P_T, d) = \sum_{k=1}^{K} \Delta f \log_2 \left[1 + \frac{P_T}{\zeta_B L(f_k, d) T_{tot}(f_k, d) \Delta f} \right],
\tag{24}
$$

where Δf is the width of sub-band and f_k is the center frequency of the k-th sub-band. Substituting (17) and (22) into (24), we obtain (18) and thus proving the above lemma. ∎

Corollary 1. *When $h_T \ll d$, $h_R \ll d$, $d \to 0$ and $G_T = G_R = 1$, the channel capacity of a nanocommunication system can be given by*

$$
\begin{aligned}
C(P_T, d) \approx \sum_{k=1}^{K} \Delta f \log_2 &\left[1 + \frac{P_T h_T^2 h_R^2}{\zeta_B d^4 \Delta f} \right. \\
&\left. \times \frac{1}{T_S + (T_S + T_0)\kappa(f_k)d} \right].
\end{aligned}
\tag{25}
$$

Proof: As $h_T \ll d$, $h_R \ll d$ and $d \to 0$, applying Maclaurin serie [22, eq. (0.318.2)], it can be approximated that

$$
\sin^2 \left(\frac{2\pi h_T h_R f_k}{\zeta_L d} \right) \approx \left(\frac{2\pi h_T h_R f_k}{\zeta_L d} \right)^2, \tag{26}
$$

$$
\prod_{i,g} e^{\kappa^{(i,g)}(f_k)d} \approx 1 + \sum_{i,g} \kappa^{(i,g)}(f_k)d = 1 + \kappa(f_k)d. \tag{27}
$$

Substituting (26) and (27) into (18) with the assumption of $G_T = G_R = 1$, the corollary is proved. ∎

It can be deduced from the above channel model that, the total path loss of electromagnetic signal transmission from between a transmitting and receiving pair has both DPL and MAA components which drastically reduce the performance and reliability of WiNoCs as will be shown latter in Section VI. Consequently, it is crucial to explore alternative communication fabric that is able transmit wireless signals with minimum losses.

VI. SIMULATION RESULTS

To understand the effect of the wireless channel on the total reliability of WiNoCs, the performance evaluation of the mm-wave wireless channel is carried out by investigating the channel model proposed in Section IV. We compare with conventional channel model where signals are transmitted over
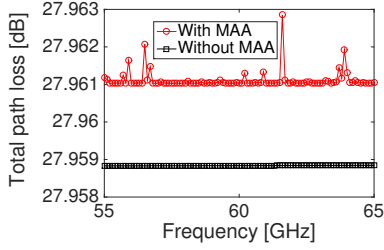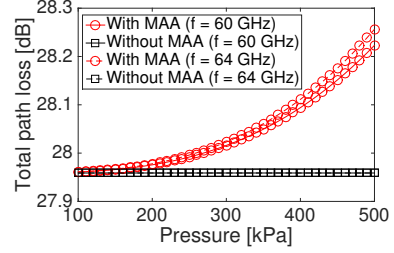
Fig. 4. Total path loss versus frequency.

Fig. 5. Total path loss versus ambient pressure at different frequencies.

Fig. 6. Total path loss versus distance between mm-Wave antennas at different frequencies.eps

pure air with no MAA (e.g. two-ray channel model in [20])[2].

The simulation is implemented in MATLAB and the parameters of various gas compositions are obtained from the HITRAN database [18]. The impacts of the transmission medium and various channel environment parameters on the performance of mm-Wave WiNoC in terms of path loss and channel capacity are evaluated with respect to different channel modeling approaches. First, we investigate the impacts of antenna transmission frequency on the wireless channel model. Fig. 4 plots the variation of the total path loss (i.e. L) of the two considered channel models with transmission frequency at $\mathcal{C}_\mathcal{T}$. Two cores $\mathcal{C}_\mathcal{T}$ and $\mathcal{C}_\mathcal{R}$ (i.e. d_C) are implemented on a chip with a die size of 20mm^2 and the height (i.e. h) of 1mm. The distance between $\mathcal{C}_\mathcal{T}$ and $\mathcal{C}_\mathcal{R}$ (i.e. d) is set to be 0.1mm, satisfying $d < d_C\sqrt{2}$. Each core deploys a zigzag antennas having an elevated height of 0.02mm (i.e. $h_T = h_R = 0.02$mm). The transmission frequency of the antennas (i.e. f) is assumed to vary in the range from 55GHz to 65GHz. The system electronic noise temperature (i.e. T_S) is 296 K and the ambient pressure applied on the chip (i.e. p) is 1atm.

It can be observed in Fig. 4 that the practical channel model for WiNoCs results in a higher total path loss compared to the conventional channel model. Also, the total path loss is shown to not monotonically increase at the GHz frequency band due to the fact that the MAA is caused by isotopologues of gases having various absorption coefficients at various frequencies. For example, the MAA causes a very high path loss at about 61.6GHz. These observations confirm the statements in Remarks 1 and 2 regarding the effectiveness of the proposed channel model with environment-aware property.

Taking the ambient pressure of WiNoCs into consideration, Fig. 5 plots the total path loss of various channel models versus the ambient pressure (i.e. p in kPa[3]) applied on the chip package. It can be seen in Fig. 5 that the total path loss in the conventional channel model is independent of the ambient pressure. However, the total path loss in the proposed channel
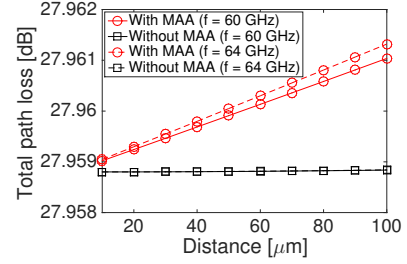
model for practical WiNoC is shown to exponentially increase as the ambient pressure increases, which confirms the claim of the exponentially increased total path loss over the ambient pressure in Remark 2. Considering the impacts of distance between two cores on the performance of WiNoC, in Fig. 6, the total path loss of various channel models is plotted. We consider the transmission distance between $\mathcal{C}_\mathcal{T}$ and $\mathcal{C}_\mathcal{R}$ (i.e. d) with respect to two values of frequency $f = 60$GHz and $f = 64$GHz. The distance d is assumed to vary in the range $[10 : 100]\mu s$ and the other simulation parameters are similarly set as in Fig. 4. It can be observed that the total path loss in both the proposed and the conventional channel models increases as the distance increases, which could be straightforwardly verified from the path loss expression in (17). However, there is only a slightly increase of the path loss in the conventional model at the GHz frequency band, while such increase is shown to be significant with a much higher path loss in the proposed channel model, which is in fact caused by the consideration of the MAA to reflect the practical WiNoC. We
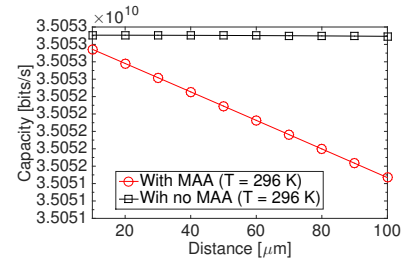

Fig. 7. Channel capacity versus distance between two antennas.

investigate the impacts of MAA in the proposed channel model on the achievable channel capacity of WiNoCs. Fig. 7 plots the channel capacity against the distance between two cores $\mathcal{C}_\mathcal{T}$ and $\mathcal{C}_\mathcal{R}$. Similarly, two channel models including the proposed

---

[2]In our model, the parameterizable medium compositions consist of water vapour (which could also an effect of emerging liquid cooling technology), carbon dioxide, oxygen, nitrogen, ozone, molecular hydrogen, nitrous oxide, methane, dioxygen, nitrogen oxide, sulfur dioxide, acetylene, ethane, ethylene, methanol, hydrogen cyanide, chloromethane, hydroxyl radical, hydrogen chloride, chlorine monoxide, carbonyl sulfide, formaldehyde, hypochlorous acid, hydrogen peroxide, phosphine, carbonyl fluoride, sulfur hexafluoride, hydrogen sulfide, formic acid, hydroperoxyl radical, chlorine nitrate, nitrosonium ion, hypobromous acid, bromomethane, acetonitrile, carbon tetrafluoride, diacetylene, cyanoacetylene, carbon monosulfide, sulfur trioxide.

[3]Note that 1atm = 101.325kPa

and the conventional models are considered for comparison and the parameters are set as in Fig. 6. The antennas are assumed to operate at frequency $f = 60\text{GHz}$. As shown in Fig. 7, the channel capacity in the proposed channel model for the practical WiNoCs is lower than that in the conventional channel model, even when the distance between two cores is less than 0.01mm. This observation can be intuitively verified through the impacts of the transmission distance on the total path loss.

VII. Conclusion And Future Work

In this paper, we have proposed an efficient channel model for WiNoCs, operating in the GHz band, which accounts for the on-chip constraints. It has been shown that MAA has a considerable effect on the reliability of WiNoCs. Specifically, the MAA has been shown to cause a very high path loss at certain frequencies rather than monotonically increasing over the frequencies as in the conventional channel model. Additionally, the total path loss has been shown to exponentially increases as the ambient pressure applied on the chip increases. Moreover, the total path lose increases as the distance between two cores increases which increases the number of erroneous transmissions in WiNoCs. Unlike conventional approach, our experimental evaluation reveals that a practical channel model for the wireless layer of WiNoCs have a lower channel capacity, which reflects the increased BER and reduced reliability of overall system at the GHz band, even when the separation distance between two antennas is very small (less than 0.01 mm). Future work involves the evaluation of the latency, area and power consumption overhead of novel coding techniques for improving the reliability of WiNoCs.

References

[1] R. Marculescu, U. Ogras, L.-S. Peh, N. Jerger, and Y. Hoskote, "Outstanding research problems in noc design: System, microarchitecture, and circuit perspectives," *IEEE on Computer-Aided Design of Integrated Circuits and Systems*, vol. 28, no. 1, pp. 3 –21, 2009.

[2] M. O. Agyeman, A. Ahmadinia, and A. Shahrabi, "Heterogeneous 3d network-on-chip architectures: Area and power aware design techniques," *Journal of Circuits, Systems, and Computers*, vol. 22, no. 4, 2013.

[3] R. Marculescu and P. Bogdan, "The chip is the network: Toward a science of network-on-chip design," *Foundations and Trends in Electronic Design Automation*, vol. 2, no. 4, pp. 371–461, 2009.

[4] P. Bogdan, "Mathematical modeling and control of multifractal workloads for data-center-on-a-chip optimization," in *Proceedings of the 9th International Symposium on Networks-on-Chip*, ser. NOCS '15, 2015, pp. 21:1–21:8.

[5] M. O. Agyeman, W. Zong, J. Wan, A. Yakovlev, K. Tong, and T. S. T. Mak, "Novel hybrid wired-wireless network-on-chip architectures: Transducer and communication fabric design," in *Proceedings of the 9th International Symposium on Networks-on-Chip, NOCS*, 2015, pp. 32:1–32:2.

[6] Y. P. Zhang, Z. M. Chen, and M. Sun, "Propagation mechanisms of radio waves over intra-chip channels with integrated antennas: Frequency-domain measurements and time-domain analysis," *IEEE Transactions on Antennas and Propagation*, vol. 55, no. 10, pp. 2900–2906, 2007.

[7] X. Dong and Y. Xie, "System-level cost analysis and design exploration for three-dimensional integrated circuits (3d ics)," in *Asia and South Pacific Design Automation Conference (ASP-DAC)*, 2009, pp. 234 – 241.

[8] M. O. Agyeman and A. Ahmadinia, "Optimised application specific architecture generation and mapping approach for heterogeneous 3d networks-on-chip," in *International Conference on Computational Science and Engineering (CSE)*, 2013, pp. 794–801.

[9] M. Opoku Agyeman, A. Ahmadinia, and N. Bagherzadeh, "Performance and energy aware inhomogeneous 3d networks-on-chip architecture generation," *IEEE Transactions on Parallel and Distributed Systems*, vol. PP, no. 99, pp. 1–1, 2015.

[10] M. Opoku Agyeman, K.-F. Tong, and T. Mak, "Towards reliability and performance-aware wireless network-on-chip design," in *IEEE International Symposium on Defect and Fault Tolerance in VLSI and Nanotechnology Systems (DFTS)*, 2015, pp. 205–210.

[11] S. Deb, A. Ganguly, P. Pande, B. Belzer, and D. Heo, "Wireless noc as interconnection backbone for multicore chips: Promises and challenges," *IEEE Journal on Emerging and Selected Topics in Circuits and Systems*, vol. 2, no. 2, pp. 228–239, 2012.

[12] C. Xiao, Z. Huang, and D. Li, "A tutorial for key problems in the design of hybrid hierarchical noc architectures with wireless/rf," *Smart CR*, no. 6, pp. 425–436.

[13] A. Ganguly, P. Pande, B. Belzer, and A. Nojeh, "A unified error control coding scheme to enhance the reliability of a hybrid wireless network-on-chip," in *IEEE International Symposium on Defect and Fault Tolerance in VLSI and Nanotechnology Systems (DFT)*, 2011, pp. 277–285.

[14] S. Lee, S. Tam, I. Pefkianakis, S. Lu, M. F. Chang, C. Guo, G. Reinman, C. Peng, M. Naik, L. Zhang, and J. Cong, "A scalable micro wireless interconnect structure for cmps," in *Annual International Conference on Mobile Computing and Networking MOBICOM*, 2009, pp. 217–228.

[15] V. Vijayakumaran, M. P. Yuvaraj, N. Mansoor, N. Nerurkar, A. Ganguly, and A. Kwasinski, "Cdma enabled wireless network-on-chip," *J. Emerg. Technol. Comput. Syst.*, vol. 10, no. 4, pp. 28:1–28:20, 2014.

[16] D. Matolak, S. Kaya, and A. Kodi, "Channel modeling for wireless networks-on-chips," *IEEE Communications Magazine*, vol. 51, pp. 180–186, 2013.

[17] M. Ravenstahl and M. Kopp, "Application brief: Ansys hfss for ecad, ansys," 2013.

[18] L. Rothman, I. Gordon, Y. Babikov, A. Barbe, D. C. Benner, P. Bernath, M. Birk, L. Bizzocchi, V. Boudon, L. Brown, A. Campargue, K. Chance, E. Cohen, L. Coudert, V. Devi, B. Drouin, A. Fayt, J.-M. Flaud, R. Gamache, J. Harrison, J.-M. Hartmann, C. Hill, J. Hodges, D. Jacquemart, A. Jolly, J. Lamouroux, R. L. Roy, G. Li, D. Long, O. Lyulin, C. Mackie, S. Massie, S. Mikhailenko, H. Mller, O. Naumenko, A. Nikitin, J. Orphal, V. Perevalov, A. Perrin, E. Polovtseva, C. Richard, M. Smith, E. Starikova, K. Sung, S. Tashkun, J. Tennyson, G. Toon, V. Tyuterev, and G. Wagner, "The {HITRAN2012} molecular spectroscopic database," *Journal of Quantitative Spectroscopy and Radiative Transfer*, vol. 130, no. 0, pp. 4 – 50, 2013.

[19] T. G. Kyle, *Atmospheric transmission, emission and scattering*. New York: Pergamon, 1991.

[20] T. Rappaport, *Wireless Communications: Principles and Practice*. Prentice Hall PTR, 2001.

[21] R. M. Goody and Y. L. Yung, *Atmospheric Radiation: Theoretical basis*. Oxford University Press, 1989.

[22] I. S. Gradshteyn and I. M. Ryzhik, *Table of Integrals, Series, and Products*. Academic Press, 2007.